

FIG. 1. **Experimental observations of an annealed Ni film on sapphire.** **a**, Atomic Force Microscopy (AFM) topography image of a Ni film on sapphire after heat treatment, showing sunken grains with (green arrow) and without (red arrow) an elevated ridge around the edges. **b**, A linear topographic profile across the hole indicated using a green arrow in **a** showing a Ni ridge at the perimeter of the sunken grain. **c**, 3-D image of the same hole showing an elevated ridge surrounding the sunk grain. **d**, A linear topographic profile across the hole indicated using the red arrow in **a** showing no measurable ridge formation. **e**, 3-D image around the same hole showing a hole left by grain sinking.

have $\langle 111 \rangle$ surface normals with two in-plane orientations (rotated by 60° about the normal with respect to one another); this is referred to as a *maze* microstructure. We observed that the grain surfaces are flat, except for the presence of ridges and/or grooves at some GBs and holes within some of the grains [23] (see Fig. 1a).

The presence of isolated holes, not connected to GBs, is a clear indication that isolated/embedded grains (see Fig. 1a) sink and disappear, leaving through-thickness holes. These holes form in an early stage of solid-state dewetting. The hole indicated by the green arrow in Fig. 1a is surrounded by a slightly elevated ridge (see Fig. 1b,c). Integrating the profile around this hole from the AFM topography reveals that the volume contained in the ridge is $\sim 0.5 \times 10^{-2} \mu\text{m}^3$, while the volume of the material removed to form the hole is $\sim 2X$ as large. The “sunken” grain indicated by the red arrow in Fig. 1a shows no such ridges (Fig. 1d,e). In the classic theory of GB grooving [24], all of the material removed around the GB goes into the ridge. Where did the missing Ni atoms go? How did these holes form?

We suggest that the missing Ni in the grooving/hole formation, diffuses down the GB and then along the Ni/sapphire interface (see Fig. 2a). For this process to continue, Ni diffusion along the Ni/sapphire interface must be rapid. In this case, the film surrounding the sunken grain must thicken by the accretion of Ni atoms

at the Ni/sapphire interface [23]. Similar homogeneous thickening of a metal film associated with material redistribution along the metal-ceramic interface was recently reported in Al/sapphire [21].

We test this hypothesis by developing a short-circuit diffusion model that describes the surface topography evolution of a thin metal film on a ceramic substrate via simultaneous surface, GB, and interface metal diffusion (see Fig. 2a and Supplementary Information, SI for details). Numerical solution of the evolution of the surface profile for the case of a small, axisymmetric grain of radius R_0 embedded in a continuous film is shown in Fig. 2b for three different interface diffusivities at the time when the GB groove hits the substrate (i.e., hole nucleation and onset of solid state dewetting). This figure clearly shows that interface diffusion greatly enhances the rate of hole formation and reduces the amplitude of the elevated rim demonstrating that our model is consistent with the observations.

We analyze the experimental case of Fig. 1b,c (where a small ridge forms around the sinking grain) employing reasonable values of GB and surface diffusivities for Ni via our model (see SI) in order to determine the interface diffusivity required to explain the “missing” Ni (the difference between the Ni forming the ridge and that from the sinking grain, $\Delta V = 0.5 \times 10^{-2} \mu\text{m}^3$ after a 10 minute annealing at 700°C). These experimental obser-

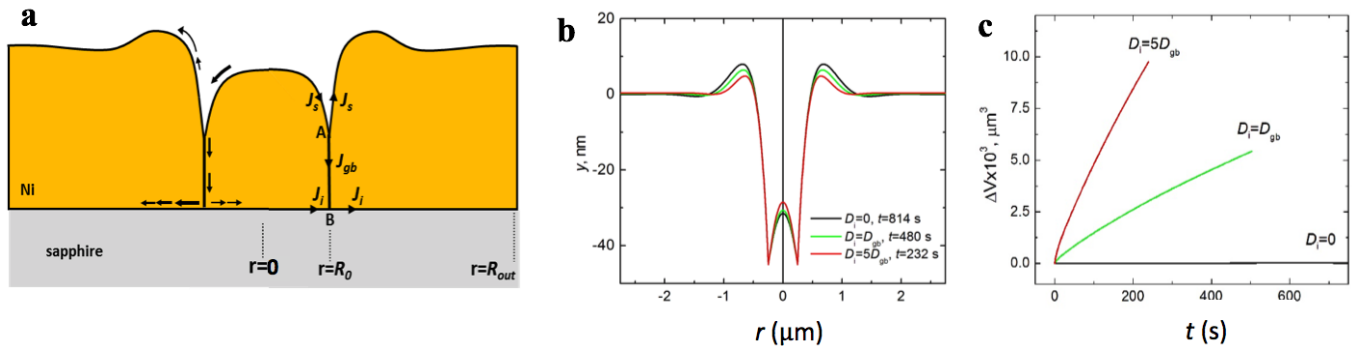


FIG. 2. **Development and results of the morphology evolution model.** **a**, The Ni/sapphire model showing Ni flux along the Ni surface (J_s), along the GB (A is the GB root position) between the sinking middle grain and the outer grain (J_{gb}), and along the Ni/sapphire interface (J_i) (B is the location of the intersection of the GB and the interface). **b**, Surface topography profiles $y(r)$ for three different interface diffusivities at the time t the GB root hits the metal/ceramic interface at 700°C. **c**, Calculated “missing” Ni volume ΔV vs. time.

vations yield $D_i \approx D_{gb}$ (for a random large angle GB in Ni [25]). We note that given the variability of GB and surface diffusivity with bicrystallography and the uncertainty in the experimental measurements, we consider this to be an “order of magnitude” estimate.

This interface diffusivity is surprisingly large given that this metal/ceramic interface is nearly coherent and the strong bonding between this metal and ceramic. We now address the question, “why is this interface diffusivity so large?” and, “is this a generic finding for all metal/ceramic interfaces?”

First-principles modeling of point defects

To understand fast transport along the Ni/sapphire interface, we first focus on point defect formation energetics using density functional theory (DFT) (to account for the complex bonding at the interface). Transmission electron microscopy examinations of the Ni/sapphire interface established two distinct orientation relationships. These are M1: Ni(111)[1 $\bar{1}$ 0]||Al₂O₃(0001)[11 $\bar{2}$ 0] and M2: Ni(111)[1 $\bar{2}$ 1]||Al₂O₃(0001)[11 $\bar{2}$ 0] [26, 27] (which is rotated by 30° about the surface normal from M1) [27]. Perfect interface coherency demands that Ni is biaxially strained -2.8% for M1 and +12.3% for M2. We focus on the less strained M1 interface (the M2 interface will have a much higher interface energy associated with a high density of misfit dislocations). The O-terminated Al₂O₃/Ni interface is shown in Fig. 3a; the Al₂O₃ may also be terminated by one or two Al atom planes. Examination of Fig. 3b shows that the 2Al-terminated and O-terminated interfaces are stable over a wide range of oxygen chemical potentials; at high (low) p_{O_2} the O (2Al)-terminated Ni/Al₂O₃ interfaces will be thermodynamically stable (the maximum and minimum $p_{O_2}^{\max}$ and $p_{O_2}^{\min}$ are set by Ni oxidation and Al₂O₃ reduction - see SI). For each sapphire termination, the Ni (111) termination may be A, B or C, corresponding to the classical description of the (111) plane stacking of FCC materials (i.e., ...ABCABC...) - these 3 terminations also represent Ni

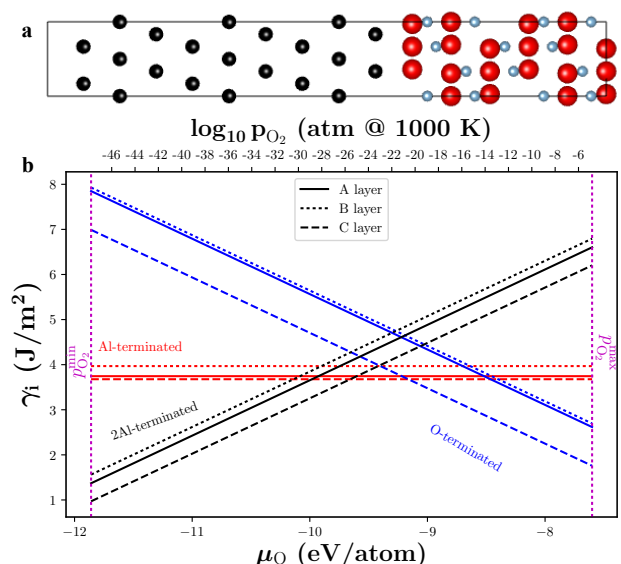


FIG. 3. **DFT prediction of the M1 Ni(111)[1 $\bar{1}$ 0]||Al₂O₃(0001)[11 $\bar{2}$ 0] interface energy.** **a**, Unrelaxed, atomistic model of the (C-terminated) Ni/(O-terminated) sapphire interface. Ni, Al and O are shown in black, blue and red. **b**, Interface energy of the Ni/sapphire interface considering the three Ni translations and the three sapphire terminations.

crystal shifts parallel to the interface (see SI). Our DFT calculations show that the termination C-Ni/sapphire is most stable for both 2Al and O sapphire terminations. For the O-terminated sapphire interface, the C-Ni termination corresponds to placing a Ni atom at the same position that would be occupied by an Al atom in perfect sapphire [28].

Since diffusion in Ni is vacancy-controlled [29], we determine vacancy formation energies in Ni and α -Al₂O₃ as a function of distance d from the Ni/sapphire interface and p_{O_2} ; e.g., the formation energy of the neutral

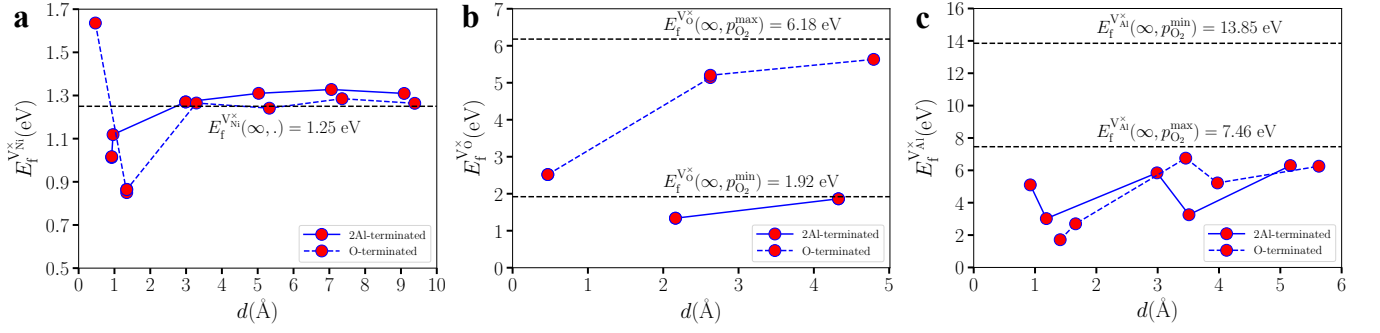


FIG. 4. **Variation of vacancy formation energies** ($E_f^{V_{Ni}^{\times}}$, $E_f^{V_{O}^{\times}}$, $E_f^{V_{Al}^{\times}}$) **versus distance from the interface d .** **a**, Ni vacancy formation energy for both O-terminated and 2Al-terminated sapphire interfaces. The horizontal dashed line represents the vacancy formation in bulk strained Ni (corresponding to M1 epitaxy). **b**, Neutral O vacancy formation energy for both the terminations. For the O-terminated case, the bulk O vacancy formation energy (dashed line) is for $p_{O_2}^{\max}$ and at $p_{O_2}^{\min}$ for the 2Al-termination. **c**, Neutral Al vacancy formation energy for both the terminations. The bulk Al vacancy formation energies for the O-terminated and 2Al-terminated cases are for $p_{O_2}^{\max}$ and $p_{O_2}^{\min}$.

O-vacancy (i.e., formed by removing an O atom and all of its electrons) in Al_2O_3 is denoted by $E_f^{V_{O}^{\times}}(d, p_{O_2})$ in Kröger-Vink notation [30]. At the metal-ceramic interface, we expect the net charge on point defects to be near zero since the Fermi level of the system will be pinned to that of the metal [31]. Hence, unlike in bulk ceramics (see SI), neutral point defects may be formed near both sides of the interface.

We first calculate neutral vacancy formation energies in bulk Ni and $\alpha-Al_2O_3$ ($d=\infty$); $E_f^{V_{Ni}^{\times}}(\infty, \cdot)$ ($p_{O_2} = \cdot$ indicates p_{O_2} -independence), $E_f^{V_{Al}^{\times}}(\infty, p_{O_2})$ and $E_f^{V_{O}^{\times}}(\infty, p_{O_2})$. $E_f^{V_{Ni}^{\times}}(\infty, \cdot) = 1.51$ eV (unstrained, close to the experimentally found value of 1.6 eV [32]) or 1.25 eV (strained to M1 epitaxial relationship, -2.8%). Similarly, since Schottky defects are more prevalent than Frenkel defects in $\alpha-Al_2O_3$ [33, 34], we focus on Al and O vacancies on the sapphire side of the interface. For bulk sapphire, the neutral vacancy formation energies depend on oxygen partial pressure; on oxygen sites $E_f^{V_{O}^{\times}}(\infty, p_{O_2}^{\min}) = 1.92$ eV and $E_f^{V_{O}^{\times}}(\infty, p_{O_2}^{\max}) = 6.18$ eV. The neutral Al vacancy formation energy is $E_f^{V_{Al}^{\times}}(\infty, p_{O_2}^{\min}) = 13.85$ eV and $E_f^{V_{Al}^{\times}}(\infty, p_{O_2}^{\max}) = 7.46$ eV (see SI Fig. 3). These vacancy formation energies suggest that near the interface the equilibrium vacancy concentration in Ni is much higher than either Al or O vacancies in sapphire.

Figure 4 shows the neutral Ni, Al, and O vacancy formation energies as a function of distance d from the O-terminated sapphire and 2Al-terminated sapphire/C-plane Ni interfaces. For the O-terminated sapphire interface, the Ni vacancy formation energy $E_f^{V_{Ni}^{\times}}(d, \cdot)$ drops from its bulk value 1.28 eV far from the interface to 0.85 eV (i.e., 66% of the bulk value for pure Ni) two (111) Ni atomic planes from the interface. On the other hand, immediately adjacent to the sapphire in Fig. 4a, the Ni vacancy formation energy is very large, 1.64 eV, likely

because of the strong metal–oxygen bond. While removing a Ni atom from this site is not as energetically costly as removing an Al atom from bulk sapphire (the Al vacancy formation energy is 7–13 eV depending on p_{O_2}), it is higher than it would be for removing a Ni atom from a Ni crystal. The same trend also applies to the 2Al-terminated sapphire interface. Hence, the Ni vacancy formation energy is much smaller near the interface than in the Ni interior for all Ni/ $\alpha-Al_2O_3$ interfaces. This implies that the thermal concentration of Ni vacancies near the interface is much higher than elsewhere in Ni.

Figure 4b,c shows that the O and Al vacancy formation energies decrease from their bulk values as we approach the interface. For example, in the O-terminated sapphire case, the O vacancy formation energy decreases from 5.63 eV to 2.52 eV as it approaches the interface (at $p_{O_2}^{\max}$).

Similarly, $E_f^{V_{Al}^{\times}}(d, p_{O_2}^{\max})$ drops from 6.25 eV to 1.71 eV near the interface (the 2Al-terminated case is discussed in SI).

While the lowest formation energy point defect near the interface is the Ni vacancy $E_f^{V_{Ni}^{\times}} = 0.85$ eV, the third lowest is the Al vacancy in O-terminated sapphire $E_f^{V_{Al}^{\times}} = 1.71$ eV (the second lowest energy is an oxygen vacancy). In this case, however, the Al vacancy is replaced by a Ni interstitial and a vacancy on the Ni side of the interface (see Fig. 7 in SI). Hence consideration of defect complexes at the interface involving the low-formation energy defects (V_{Ni} , V_{Al}) reveals that the Ni vacancy concentration at the metal/ceramic interface is expected to be even higher than that suggested by the single point defect formation energies alone.

Interface transport

Vacancy defect-mediated diffusion is commonly characterized as $D = D_0 e^{-E_f^V/k_B T} e^{-E_m^V/k_B T}$, where the pre-exponential factor D_0 accounts for crystal structure, the effective atomic vibration frequency, interatomic separa-

tion, correlation and entropy effects, $k_B T$ is the thermal energy, E_f^V and E_m^V are the vacancy formation and migration energies respectively [35]. The arrhenius terms describe the equilibrium vacancy concentration and vacancy migration, respectively. While in ceramics, the point defect density may be modified by doping, in metals it is usually dictated by equilibrium thermodynamics (vacancies are easily produced/annihilated by dislocation climb).

Using nudged elastic band calculations [36], we determine the barrier for Ni vacancy migration (see SI) parallel to the interface (second layer) to be 0.49 eV, which is $\sim 1/2$ its bulk value. Since the Ni vacancy formation energy at this location is ~ 0.7 that in bulk Ni, our results are consistent with earlier discovered trends [37] that showed that in elemental FCC and HCP metals both the vacancy formation and migration energies scale in the same manner (linearly) with cohesive energy (i.e., the drop in the vacancy energies is related to reduced cohesion at the interface compared with bulk Ni). Combining the vacancy formation and migration results reported here, these results suggest that at, for example, half the Ni melting point, the interface diffusivity should be $\geq 10^4$ times faster than in bulk Ni. GB diffusivities in metals are typically ($10^4 - 10^6$) faster than lattice diffusion [14], which implies that metal/ceramic interface diffusivity and GB diffusivities are comparable at the same homologous temperature. Therefore, these results demonstrate that Ni transport along the Ni/sapphire interface is extraordinarily fast (relative to bulk diffusion). This conclusion is valid for both the coherent interface case analyzed here in detail and the case where the interface is semicoherent (which should be faster).

To explore the generalization of this result, we compare the formation energy of a vacancy at the metal/ceramic interface to that within the bulk metal in terms of the local bonding at these locations, as captured by the metal/ceramic work of adhesion W_{ad} and the metal surface energy γ_m . We estimate the ratio of the metal vacancy formation energy at the metal/ceramic interface to that in the bulk metal in terms of a simple, heuristic bond breaking model (see SI) as

$$\frac{E_f^{V_m^x}(0)}{E_f^{V_m^x}(\infty)} = \frac{W_{ad}}{\gamma_m}. \quad (1)$$

To test the applicability of this simple prediction, we compare it with the DFT results for FCC-Ni/ α -Al₂O₃ (as described above), FCC-Cu/ α -Al₂O₃ and HCP-Ti/ α -Al₂O₃. As shown in Table I and Fig. 5, the empirical descriptor (W_{ad}/γ_m) accurately predicts the ratio of $E_f^{V_m^x}(0)/E_f^{V_m^x}(\infty)$ to within 3% for Ti, 18% for Cu, and 10% for Ni. This is remarkable agreement given the simplicity of equation (1).

We use this descriptor to predict the ratio of the vacancy formation energy at the metal/ceramic interface for a wide range of metal/ceramic systems based upon

TABLE I. Vacancy formation energies of Ni, Cu and Ti at their interfaces with sapphire and in their bulk strained states, their ratio and the prediction as per equation (1) from 38–40.

	DFT			Descriptor
	$E_f^{V_m^x}(0)$ (eV)	$E_f^{V_m^x}(\infty)$ (eV)	$\frac{E_f^{V_m^x}(0)}{E_f^{V_m^x}(\infty)}$	$\frac{W_{ad}}{\gamma_m}$
Ni	0.85	1.25	0.68	0.62
Cu	0.25	0.56	0.45	0.37
Ti	2.00	2.19	0.91	0.94

equation(1) and using data readily available from the literature [38–43]. The resultant predictions are summarized in Fig. 5. Given the correlation between activation energy for vacancy migration and vacancy formation, we predict that metal diffusion along the interface will be faster than bulk diffusion for systems in which $E_f^{V_m^x}(0)/E_f^{V_m^x}(\infty) < 1$. Most of the metal/ceramic systems shown in Fig. 5 fall into this category, including Ni/Al₂O₃ (and Cu/Al₂O₃). For systems with $E_f^{V_m^x}(0)/E_f^{V_m^x}(\infty) \sim 1$, diffusion in the bulk and at the interface will be comparable (Ti/Al₂O₃) and for others ($E_f^{V_m^x}(0)/E_f^{V_m^x}(\infty) > 1$) interface diffusion is slower than in the bulk. The case of Ti/Al₂O₃, for which we have DFT data, is near the cusp - the interface diffusivity should be comparable with bulk diffusion in Ti. Amongst the cases shown in Fig. 5 are many metal/ceramic pairs that are commonly used across a wide range of technologies. We note that the {Cr, Mn, Au, Cu, Sn}/Al₂O₃ and that {Au, Cu, Sn, Ag, Fe, Co Pd, Ga}/SiO₂ inter-

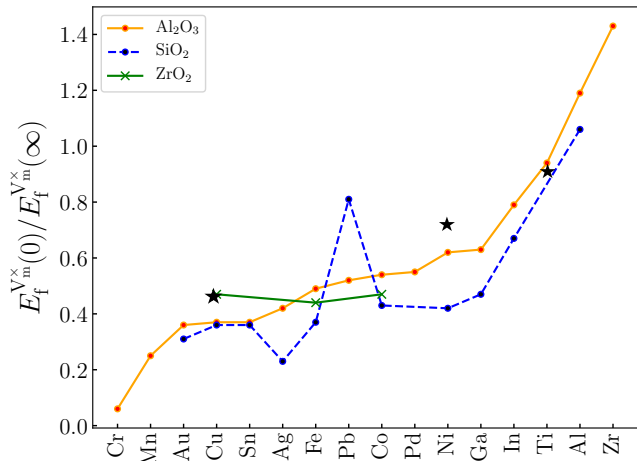


FIG. 5. **The predicted ratio of the vacancy formation energies at the metal/ceramic interface to that in the bulk metal for several metal-ceramic systems according to equation (1).** The values for γ_m and W_{ad} are from 38–43. The metals are indicated along the horizontal axis and different ceramics by the three curves. The Ni/Al₂O₃, Cu/Al₂O₃ and Ti/Al₂O₃ data (black stars) are from direct DFT calculations.

faces all show $E_f^{V_m}(0)/E_f^{V_m}(\infty) < 0.5$, suggesting that all of these interfaces will exhibit extremely fast metal transport along these interfaces. However, given that extremely fast metal atom diffusion along metal/ceramic interfaces is the rule rather than the exception, fast metal/ceramic interface diffusion should not be considered anomalous after all.

We demonstrated both experimentally and computationally that diffusion at the Ni/sapphire is surprisingly fast. Our first-principles vacancy formation and migration energy calculations demonstrate that this is a result of relatively low cohesion at this interface compared with bulk Ni. This observation suggests a simple descriptor for diffusion at the interface compared with the bulk based upon readily available experimental and/or first-principles results. Based on this descriptor, we conclude that for most metal/ceramic systems (we examined close-packed metals and sapphire, silica, zirconia), inter-

face diffusion is fast compared with the bulk and comparable with metal grain boundary diffusivities in many cases; yet there are exceptions (as determined based on interface cohesion). Systems where the metal only weakly wets (or does not wet) the ceramic, the interface diffusivity will be high; inversely, where the tendency for wetting is strong, the interface diffusivity will be low (all relative to the bulk metal). This suggests that alloying to modify wettability also affects interface diffusion kinetics. This simple result provides easily applicable guidance for material design in a wide range of applications; especially in the energy and microelectronics industries.

Methods

Methods are described in details along with statements of data availability in the online version of the paper.

-
- [1] Chih-Tang Sah. *Fundamentals of solid state electronics*. World Scientific Publishing Co Inc, 1991.
- [2] Roger C Reed. *The superalloys: fundamentals and applications*. Cambridge University Press, 2008.
- [3] Alexander Kraysberg and Yair Ein-Eli. Review on Li-air batteries—Opportunities, limitations and perspective. *Journal of Power Sources*, 196(3):886–893, 2011.
- [4] K Brandt. Historical development of secondary lithium batteries. *Solid State Ionics*, 69(3-4):173–183, 1994.
- [5] Eric Kazyak, Kevin N. Wood, and Neil P. Dasgupta. Improved cycle life and stability of lithium metal anodes through ultrathin atomic layer deposition surface treatments. *Chemistry of Materials*, 27(18):6457–6462, 2015.
- [6] T. Klinkert, B. Theys, G. Patriarche, M. Jubault, F. Donsanti, J.-F. Guillemoles, and D. Lincot. New insights into the Mo/Cu(In,Ga)Se₂ interface in thin film solar cells: Formation and properties of the MoSe₂ interfacial layer. *The Journal of Chemical Physics*, 145(15):154702, 2016.
- [7] RW Balluffi, CB Duke, LL Kazmerski, KW Mitchell, R Reifenberger, and RF Wood. Basic research needs and opportunities at the solid-solid interface: Diffusion. *Materials Science and Engineering*, 53(1):93–102, 1982.
- [8] C Scheu, Y Liu, SH Oh, D Brunner, and M Rühle. Interface structure and strain development during compression tests of Al₂O₃/Nb/Al₂O₃ sandwiches. *Journal of materials science*, 41(23):7798–7807, 2006.
- [9] Yuichi Ikuhara and Pirouz Pirouz. High resolution transmission electron microscopy studies of metal/ceramics interfaces. *Microscopy Research and Technique*, 40(3):206–241, 1998.
- [10] D. A. Shashkov and D. N. Seidman. Atomic scale studies of segregation at ceramic/metal heterophase interfaces. *Physical Review Letters*, 75:268–271, 1995.
- [11] R. S. Barnes. Diffusion of copper along the grain boundaries of nickel. *Nature*, 166(4233):1032–1033, 1950.
- [12] Magnus Garbrecht, Bivas Saha, Jeremy L. Schroeder, Lars Hultman, and Timothy D. Sands. Dislocation-pipe diffusion in nitride superlattices observed in direct atomic resolution. *Scientific Reports*, 7:46092, 2017.
- [13] N.A. Gjostein. Short circuit diffusion. In *Diffusion (ed. Aaronson, H. I.)*. American Society for Metals, Metals Park, Ohio, 1973.
- [14] Helmut Mehrer. *Diffusion in solids: fundamentals, methods, materials, diffusion-controlled processes*, volume 155. Springer Science & Business Media, 2007.
- [15] Dongwen Gan, Paul S. Ho, Yaoyu Pang, Rui Huang, Jihperng Leu, Jose Maiz, and Tracey Scherban. Effect of passivation on stress relaxation in electroplated copper films. *Journal of Materials Research*, 21(06):1512–1518, 2006.
- [16] L. Arnaud, T. Berger, and G. Reibold. Evidence of grain-boundary versus interface diffusion in electromigration experiments in copper damascene interconnects. *Journal of Applied Physics*, 93(1):192–204, 2002.
- [17] O. Kovalenko, J. R. Greer, and E. Rabkin. Solid-state dewetting of thin iron films on sapphire substrates controlled by grain boundary diffusion. *Acta Materialia*, 61(9):3148–3156, 2013.
- [18] Anna Kosinova, Oleg Kovalenko, Leonid Klinger, and Eugen Rabkin. Mechanisms of solid-state dewetting of thin Au films in different annealing atmospheres. *Acta Materialia*, 83:91–101, 2015.
- [19] Chr Minkwitz, Chr Herzig, E Rabkin, and W Gust. The inclination dependence of gold tracer diffusion along a Σ3 twin grain boundary in copper. *Acta materialia*, 47(4):1231–1239, 1999.
- [20] Kuan-Chia Chen, Wen-Wei Wu, Chien-Neng Liao, Lih-Juann Chen, and K. N. Tu. Observation of atomic diffusion at twin-modified grain boundaries in copper. *Science*, 321(5892):1066–1069, 2008.
- [21] Stefan Werner Hieke, Gerhard Dehm, and Christina Scheu. Annealing induced void formation in epitaxial Al thin films on sapphire (α-Al₂O₃). *Acta Materialia*, 140:355–365, 2017.
- [22] Stefan Werner Hieke, Benjamin Breitbach, Gerhard Dehm, and Christina Scheu. Microstructural evolution and solid state dewetting of epitaxial Al thin films on sapphire (α-Al₂O₃). *Acta Materialia*, 133:356–366, 2017.

- [23] D Amram, L Klinger, N Gazit, H Gluska, and E Rabkin. Grain boundary grooving in thin films revisited: the role of interface diffusion. *Acta Materialia*, 69:386–396, 2014.
- [24] William W Mullins. Theory of thermal grooving. *Journal of Applied Physics*, 28(3):333–339, 1957.
- [25] Sergiy V Divinski, Gerrit Reglitz, and Gerhard Wilde. Grain boundary self-diffusion in polycrystalline nickel of different purity levels. *Acta Materialia*, 58(2):386–395, 2010.
- [26] Zsolt Fogarassy, Gergely Dobrik, Lajos Károly Varga, László Péter Biró, and János L Lábár. Growth of Ni layers on single crystal sapphire substrates. *Thin Solid Films*, 539:96–101, 2013.
- [27] Hila Meltzman, Dan Mordehai, and Wayne D Kaplan. Solid–solid interface reconstruction at equilibrated Ni–Al₂O₃ interfaces. *Acta Materialia*, 60(11):4359–4369, 2012.
- [28] W Zhang, JR Smith, and AG Evans. The connection between ab initio calculations and interface adhesion measurements on metal/oxide systems: Ni/Al₂O₃ and Cu/Al₂O₃. *Acta Materialia*, 50(15):3803–3816, 2002.
- [29] Michel Barsoum and MW Barsoum. *Fundamentals of ceramics*. CRC press, 2002.
- [30] FA Kröger and HJ Vink. Relations between the concentrations of imperfections in crystalline solids. In *Solid state physics*, volume 3, pages 307–435. Elsevier, 1956.
- [31] Yee-Chia Yeo, Tsu-Jae King, and Chenming Hu. Metal-dielectric band alignment and its implications for metal gate complementary metal-oxide-semiconductor technology. *Journal of Applied Physics*, 92(12):7266–7271, 2002.
- [32] Wolfram Wycisk and Monika Feller-Kniepmeier. Quenching experiments in high purity Ni. *Journal of Nuclear Materials*, 69:616–619, 1978.
- [33] SK Mohapatra and FA Kröger. The dominant type of atomic disorder in α -Al₂O₃. *Journal of the American Ceramic Society*, 61(3-4):106–109, 1978.
- [34] Donghwa Lee, Jonathan L DuBois, and Vincenzo Lordi. Identification of the local sources of paramagnetic noise in superconducting qubit devices fabricated on α -Al₂O₃ substrates using density-functional calculations. *Physical Review Letters*, 112(1):017001, 2014.
- [35] Philippe Knauth and Harry L Tuller. Solid-state ionics: Roots, status, and future prospects. *Journal of the American Ceramic Society*, 85(7):1654–1680, 2002.
- [36] Graeme Henkelman, Blas P Uberuaga, and Hannes Jónsson. A climbing image nudged elastic band method for finding saddle points and minimum energy paths. *The Journal of chemical physics*, 113(22):9901–9904, 2000.
- [37] Thomas Angsten, Tam Mayeshiba, Henry Wu, and Dane Morgan. Elemental vacancy diffusion database from high-throughput first-principles calculations for fcc and hcp structures. *New Journal of Physics*, 16(1):015018, 2014.
- [38] Richard Tran, Zihan Xu, Donald Winston Balachandran Radhakrishnan, Wenhao Sun, Kristin A Persson, and Shyue Ping Ong. Surface energies of elemental crystals. *Scientific Data*, 3, 2016.
- [39] D Chatain, I Rivollet, and N Eustathopoulos. Adh esion thermodynamique dans les syst emes non-r eactifs m etal liquide-alumine. *Journal de Chimie Physique*, 83:561–567, 1986.
- [40] CHF Peden, KB Kidd, and ND Shinn. Metal/metal-oxide interfaces: A surface science approach to the study of adhesion. *Journal of Vacuum Science & Technology A: Vacuum, Surfaces, and Films*, 9(3):1518–1524, 1991.
- [41] Charles T Campbell. Ultrathin metal films and particles on oxide surfaces: structural, electronic and chemisorptive properties. *Surface Science Reports*, 27(1-3):1–111, 1997.
- [42] Dominique Chatain, Isabelle Rivollet, and Nicolas Eustathopoulos. Estimation du travail d’adh esion et des angles de contact dans les syst emes non r eactifs m etal-oxyde ionocovalent. *Journal de Chimie Physique*, 84:201–203, 1987.
- [43] Roberto Sangiorgi, Maria L Muolo, Dominique Chatain, and Nicolas Eustathopoulos. Wettability and work of adhesion of nonreactive liquid metals on silica. *Journal of the American Ceramic Society*, 71(9):742–748, 1988.

Acknowledgements

The authors gratefully acknowledge the support of the (AK and DJS) US National Science Foundation grant 1609267, (HB and ER) US-Israel Binational Science Foundation grant 2015680 and Israel Science Foundation grant 1628/15. Work partly performed under the auspices of US DOE by LLNL under Contract DE-AC52-07NA27344. The authors acknowledge fruitful discussions with Jian Han, Jianwei Sun, Anuj Goyal, Dor Amram, Bilge Yildiz and Mostafa Youssef, and Christoff Freysoldt.

Author contributions

A.K., E.R., D.J.S. designed the research; A.K., H.B. performed the computational and experimental research respectively; L.K., E.R. developed the diffusion model; L.K. performed the numerical calculations, M.W.F., V.L. contributed to discussions and analysis; the diffusion descriptor was proposed by A.K, E.R. and D.J.S; and A.K., H.B., E.R., D.J.S. wrote the paper.

Additional information

Supplementary information is available in the online version of the paper.

Conflict of interest

The authors declare no conflict of interest.